

J. SAWICKI*, M. DUDEK*, Ł. KACZMAREK*, B. WIECEK**, T. SWIATCZAK**, R. OLBRYCHT**

NUMERICAL ANALYSIS OF THERMAL STRESSES IN CARBON FILMS OBTAINED BY THE RF PECVD METHOD ON THE SURFACE OF A CANNULATED SCREW

ANALIZA NUMERYCZNA NAPRĘŻEŃ CIEPLNYCH W WARSTWIE WĘGLOWEJ OTRZYMANEJ W PROCESIE RF PECVD NA POWIERZCHNI WKRETA KOSTNEGO

For many years, research on carbon films has been stimulated by the need to simultaneously optimize their biological and mechanical properties and by the challenges related to their deposition on medical implants. The residual mechanical stress occurring inside deposited films is the most important mechanical parameter which leads to the total destruction of these films by cracking and peeling. In the present work, we systematically studied the effect of ion bombardment during the process of radio frequency plasma enhanced chemical vapor deposition (RF PECVD) by monitoring the temperature distribution on a cannulated screw using the infrared technique. The obtained experimental and finite element modeling (FEM) results show that stresses in carbon films deposited on a cannulated screw are quite inhomogeneous and depend on the geometry of the sample and the relative position of the studied contact area between the substrate/film interface and the surface of the film.

Keywords: RF PECVD, thermography, carbon films, residual stresses, finite element modeling

Od wielu lat prowadzone są badania mające na celu zredukowanie naprężeń, w węglowych warstwach stosowanych na implanty medyczne, bez pogorszenia własności mechanicznych i biologicznych. Niemniej jednak poznanie mechanizmów wywołujących naprężenia wymaga szczegółowej analizy numerycznej. Wysoka wartość naprężeń mechanicznych występujących w osadzonych warstwach prowadzi poprzez pękanie i odwarstwienie do ich całkowitego zniszczenia, co znacząco ogranicza praktyczne wykorzystanie warstw węglowych. W prezentowanej pracy, przeanalizowano wpływ bombardowania jonów podczas procesu plazmochemicznego (RF PECVD) na rozkład temperatury na powierzchni śruby ortopedycznej przy użyciu kamery termowizyjnej. Przeprowadzone eksperymenty i uzyskane rezultaty modelowania (MES) pokazały, że naprężenia w warstwach węglowych osadzonych na śrubie ortopedycznej są niejednorodne i zależą od rzeczywistej powierzchni styku pomiędzy podłożem a powłoką jak i geometrii samej próbki.

1. Introduction

The last decade has seen an increased interest in the surface modification of medical implants by applying different methods [1-3]. Carbon films (mainly diamond-like carbon – DLC) fabricated on medical implants by radio frequency plasma enhanced chemical vapor deposition (RF PECVD) have become one of the most intensively investigated options [4-8]. In this technique, the self-bias voltage of the substrate determines the structure and properties of the fabricated films. The square of the self-bias voltage in a specific reactor is proportional to the RF power and inversely proportional to the pressure in the system [9, 10]. The varying bias of the substrate not only affects the phenomena taking place on the surface of the growing film (in particular by increasing the substrate temperature), but it also influences the fragmentation of precursor molecules in the plasma [11].

Residual stresses include intrinsic stress (which arises during film growth) and thermal stress caused by the dif-

ferences in thermal expansion coefficients between the film and the substrate. For films fabricated using the RF PECVD technique, the value of the intrinsic stress is directly correlated with the fraction of sp^3 carbon atoms, which is in turn affected by the configuration of deposition parameters [9, 12]. High stress levels have several consequences as far as coating performance is concerned. In particular, a strong driving force is required to detach the coated elements, particularly if the film is relatively thick [9, 13].

Several techniques, including X-ray and wafer curvature methods, have been applied to measure thin film stress values and to discover the mechanisms causing thin film deformation. However, in most cases these measurements have been limited to simple test structures. Furthermore, it is impossible to experimentally determine the exact stress distribution within a material. Yet, since it is useful to determine local stress distribution in complex structures, extensive finite element method (FEM) modeling was used in the study. This method provides us with the temperature distribution on the surface of a sample.

* INSTITUTE OF MATERIAL SCIENCE AND ENGINEERING, TECHNICAL UNIVERSITY OF ŁÓDŹ, 90-924 ŁÓDŹ, 1/15 STEFANOWSKIEGO STR., POLAND

** INSTITUTE OF ELECTRONICS TECHNICAL UNIVERSITY OF ŁÓDŹ, 90-924 ŁÓDŹ, 211/215 WOLCZANSKA STR., POLAND

Thermography enables real-time local temperature measurement during the RF PECVD process. By using this infrared imaging technique, some functional characteristics of DLC film can be determined. The principle of thermography is based on the measurement of infrared radiation with an IR camera, taking into consideration the emissivity values of the measured objects and surfaces.

In the first part of the paper, temperature distribution on the surface of a cannulated screw was measured by an infrared camera at various parameters of the ion etching process. In the second part, the distribution of thermal stress was calculated on the basis of temperature measurement results using FEM and ANSYS software.

2. Experimental methods

The first step of the study was to measure temperature distribution in a cannulated screw made of AISI 316L steel during a radio frequency (RF, 13.56 MHz) plasma discharge in a vacuum system which is described in detail elsewhere [14, 15]. The sample was placed on a special stand in the center of an RF water-cooled electrode (cf. Fig. 1). The walls of the chamber acted as a second electrode. The temperature of the sample during the RF discharge was monitored through a silicon window with an infrared camera. The experiments were carried out for different methane and argon mixtures, with the working pressure varying from 5 Pa to 70 Pa. The power supplied to the electrode was in the range of 0.1-1.3 kW. Thereby, the value of the negative self-bias voltage changed from 300 to 800 V.

The infrared camera used in this study was a Titanium (Cedip Infrared Systems Corporation) with an InSb infrared detector and an integrated Stirling cooler. Detailed information about this IR camera is presented in Table 1.

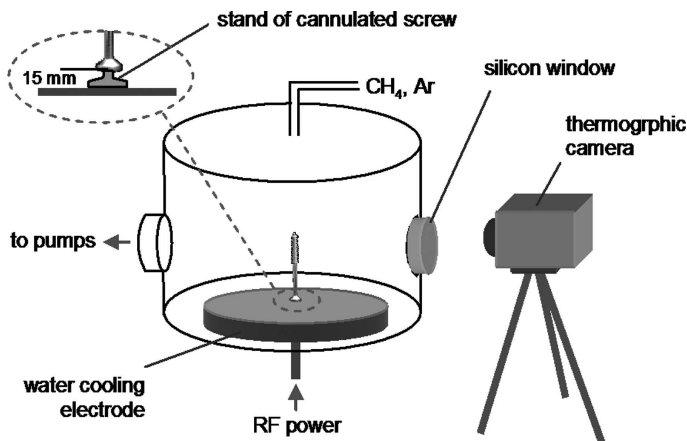


Fig. 1. Scheme of the monitoring system used to measure temperature distribution during the RF PECVD process; a cannulated screw is placed on the RF electrode on a steel stand

The second step of the study was to analyze thermal stress distribution in the sample with the carbon film. Based on the quasi-axial symmetry of the cannulated screw (shown in Fig. 2a) a two-dimensional discrete model of the sample was prepared using ANSYS software. The mesh size was decreased from 50 μm in the center of the sample to 25 μm near

its surface (Fig. 2b) to take into consideration the influence of film thickness on stress distribution. The total number of elements was about 0.5 million.

TABLE 1
Parameters of the IR camera used to measure the surface temperature of the sample during an RF plasma discharge

Parameters	Details
temperature range	5 °C to 520 °C
Resolution	640 512 pixels (25 μm pitch)
infrared wavelength	3 μm – 5 μm
shutter speed	10 μs – 100 ms
frame rate	5 – 380 Hz
noise equivalent temperature	17 mK at 20 °C

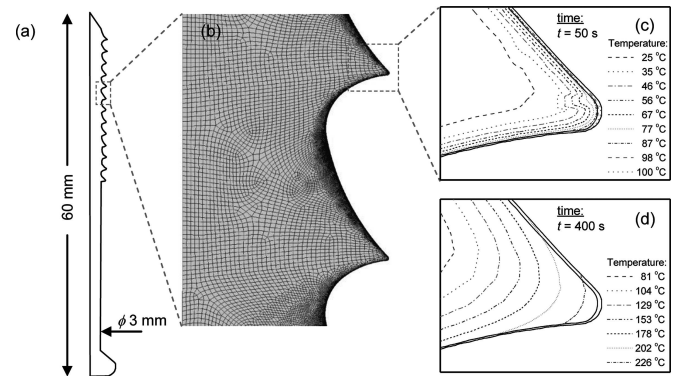


Fig. 2. Cross-section of the cannulated screw (a) and enlargement of three threads with the mesh used during the FEM analysis (b); sample temperature distribution maps for the selected thread corresponding to 50 s (c) and 400 s (d) of the RF discharge process

A simulation of the temperature distribution in the sample, consistent with the RF discharge process, was performed with a simple model based on convective heat transfer between a solid and a moving fluid:

$$Q = hAdT \quad (1)$$

where Q [W] is heat transfer per unit time, A is the heat transfer area of the surface (m^2); h [$\text{W m}^{-2} \text{K}^{-1}$] is the convection heat transfer coefficient of the process, dT [K] is the temperature difference between the surface and the bulk fluid.

In this way, we analyzed a cannulated screw submerged in warm gas and cooled by water flowing inside the electrode. Analysis was carried out using the element Plane 77 (a quadrilateral version of a 2-D 8-node thermal element with one degree of freedom, which is the temperature at each node) and the value of the convection heat transfer coefficient in the range shown in Table 2 (left column). To simplify the model, authors decided that radiation phenomena could be neglected in this case. Hence, it was easy to simulate the temperature values of the sample.

Analysis of thermal stress distribution during cooling was carried out using the element Plane 82 (a quadrilateral version of a 2-D 8-node structural element with two degrees of freedom at each node: translations in the nodal x and y directions) and the physical constants shown in Table 3.

TABLE 2

Values of the convection heat transfer coefficient used in the numerical analysis for the simulation of the temperature distribution in the sample

	$h[\text{W m}^{-2} \text{K}^{-1}]$	
	initial range	chosen value
gas	10 – 100	55
water	500 – 10000	1000

TABLE 3

Physical constants used in the numerical simulation of stress distribution

	steel	coating
Young module [GPa]	193	150
Poisson ratio	0.3	0.2
Thermal expansion coefficient [K^{-1}]	$17 \cdot 10^{-6}$	$2.3 \cdot 10^{-6}$

3. Results and discussion

Reliable temperature measurement with a thermal camera required the object emissivity value to be constant during the whole plasma process. In our case, during thin film deposition experiments, the emissivity value of the substrate surface changed with film growth. This means that a full analysis of the temperature evolution of the sample during the RF PECVD process could not be performed for a methane plasma, which was used to deposit DLC film on a cannulated screw. Therefore, the temperature of the sample was measured over time for two parameters of argon discharge – Fig. 3 shows sample temperature maps of the screw surface at various time instants during an argon RF glow discharge.

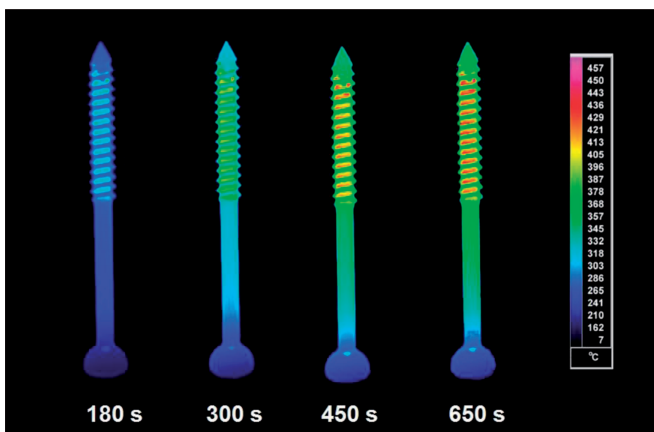


Fig. 3. Sample temperature maps at various time instants of an RF discharge; an argon discharge at 8 Pa and 800 V RF bias

Energy transfer took place between the plasma and the surface of the cannulated screw. The substrate was heated (Fig. 4), and after a certain time it reached a thermal equilibrium at the selected point of the screw. A balance of energy gain from plasma processes and energy losses determined this steady state. Energy was transferred from the substrate surface

by convection to the gas, and by radiation and conduction along the sample to the electrode.

Fig. 4 shows a profile of surface temperature distribution as a function of distance from the electrode (along the longitudinal axis of the screw) and the time of RF glow discharges for two different values of argon pressure (Fig. 4a – 8 Pa and Fig. 4b – 40 Pa) at the same self-bias voltage (800 V).

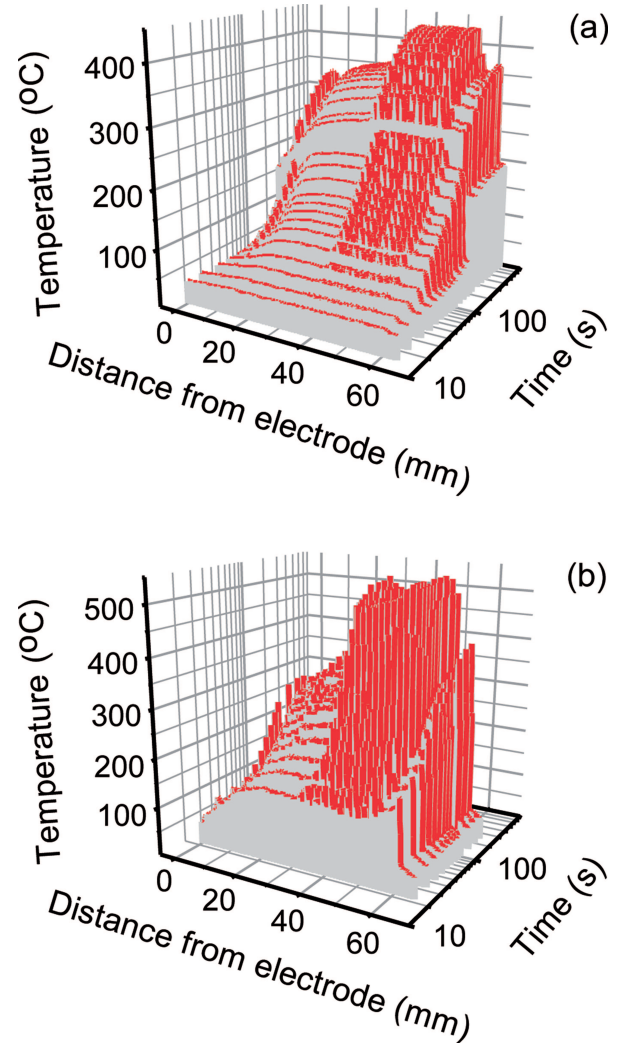


Fig. 4. Profiles of cannulated screw surface temperature during an argon discharge as a function of process time; measurement was carried out under the following external conditions: 8 Pa and 800 V RF bias (a) and 40 Pa and 800 V RF bias (b)

A comparison of temperatures for these two plasma conditions shows that in the second case the temperature stabilized at a higher value than under the lower pressure. Since the self-bias voltage was constant in both cases, the surface temperature strongly depends on the RF power supplied to the electrode.

The influence of the supplied power and pressure on plasma parameters in front of the substrate was investigated by Woodworth et al. [16]. Studies on total ion flux and mean ion energy at different pressures and various RF power values in an inductively coupled argon plasma have shown that energy flux density mainly depends on the supplied power, and less so on the pressure. This result is consistent with our measure-

ments of the temperature of the substrate surface affected by energy flux density.

The authors also considered a scenario involving changes in the temperature of the cannulated screw surface (described in Fig. 4), which occur during the deposition of DLC films. The properties of those films are strongly dependent on the surface temperature. In the case of films deposited by the RF PECVD method during a methane discharge, Keudell and Jacob's observed a shift from deposition to erosion at a substrate temperature of 225°C, and the beginning of film graphitization [17]. Fig. 4b shows that under a relatively high pressure and surface RF bias, the surface temperature at the selected point of the cannulated screw reached 500°C. This means that at these points the film was thinner. By limiting the substrate temperature to 500°C, it is possible to diffuse the carbon within the austenitic phase of AISI 316L steel without the formation of chromium carbides that hamper the corrosion resistance of the material. This was demonstrated in [18-20], considering the behavior of the AISI 316L steel substrate at this temperature.

Before analysis of the thermal stress, a simulation of temperature distribution in the sample immersed in an RF plasma was performed by the simple model described above. In a numerical simulation, we found two values of h (Table 2 – right column) for which the obtained temperature distributions (not shown here) was in agreement with the experimental results obtained for an argon discharge at 8 Pa and an 800 V RF bias (Fig. 4a). Fig. 2 (c) and (d) show sample temperature distribution maps for the selected thread corresponding to 50 s and 400 s of the RF discharge process.

The simulated substrate temperature in the cannulated screw (Fig. 2) and the different thermal expansion coefficients of the system (which was composed of a thin carbon film on AISI 316L steel) were used to analyze the distribution of thermal stress during cooling. This analysis was carried out using the physical constants shown in Table 3. The thickness of the carbon film was 0.3 μm , with one exception – on the lower thread flank it varied from 0.3 μm to 0.1 μm (see Fig. 2d, where the film is marked). Thus, having a symmetrical temperature distribution on the upper and lower thread flanks (cf. Fig. 2d), we were able to analyze the influence of geometry and thickness on stress distribution using a discrete model. Finally, we considered three profiles of stress across the substrate/film system: on the upper and lower thread flanks and on the thread crest (Fig. 5).

Fig. 5a shows the profiles of longitudinal stress for a selected node in the discrete model. The maximum value of compressive stress (which results from stress accumulation on the thread crest) is observed in the second profile. Subsequently, it steadily decreases, and at the distance of 8 μm from the surface, compressive stress turns into tensile stress. The maximum tensile stress is observed at the depth of 13 μm . In the case of the first and the third profile, the maximum compressive stress is observed in the upper layer of the film and then it achieves a value close to zero in the steel substrate.

The influence of film thickness on stress distribution is emphasized in the transverse stress profiles presented in Fig. 5b. The stress in the upper layer of the film in the first and the third profile is inversely proportional to the film thickness. Thus, for a thinner film in the third profile, the stress achieves

a value of -3.7 GPa on the lower thread flank, whereas in the first profile the stress value for a film that is three times as thick is equal to -2.1 GPa. In the second profile, the transverse stress is tensile, with its maximum at a distance of 8 μm from the surface. Due to the inhomogeneity of the film thickness, the observed difference of stress values on the upper and lower thread flanks may lead to deformation of this part of the screw. If the screw were in the bone, this would cause the film to break, and thus the protection of the human body against metal ions by the DLC film would be compromised.

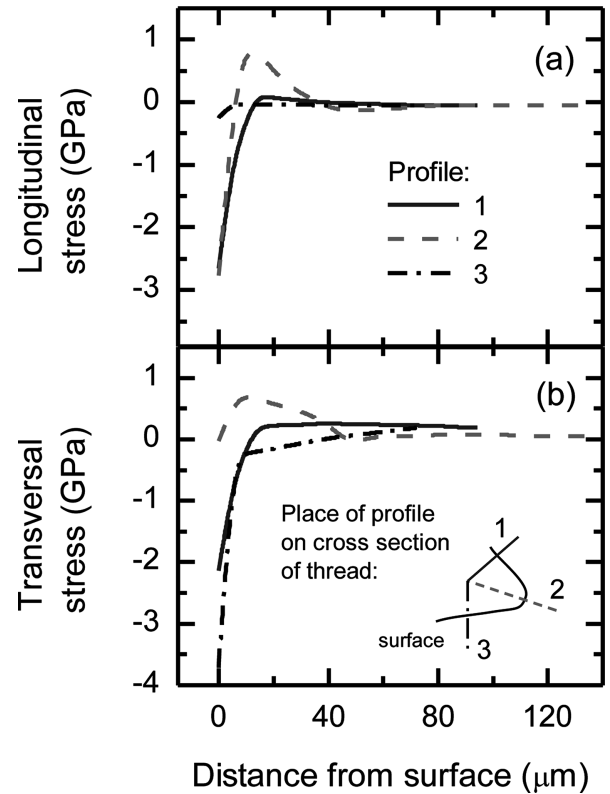


Fig. 5. Profiles of longitudinal (a) and transverse stress (b) for the studied thread (cf. Fig. 2) of the cannulated screw

4. Conclusions

In the present work, an infrared technique was successfully applied to monitor surface temperature distribution in a cannulated screw during the RF PECVD process. The obtained results were a prerequisite for developing a methodology to enable the reconstruction of the surface temperature of a sample submerged in an RF plasma, involving numerical modeling of thermal stress in a substrate/film system.

The results of finite element modeling showed that a simple model based on convective heat transfer between a solid and a moving fluid enables the reconstruction of the surface temperature of a sample, even if it has complicated geometry. The thermal stresses in the film and in the substrate are not uniform, and depend on the geometry of the sample and on the relative position of the studied contact area between the substrate/film interface and the surface of the film. The maximum compressive stress is observed in the upper layer of the thin film deposited on the thread of a cannulated screw,

and steadily decreases with the distance from the surface. The methodology described in this work can also be used to study the mechanical properties of other thin films and small volume materials.

Acknowledgements

The authors wish to thank Prof. Stanislaw Mitura (Technical University of Lodz) for stimulating discussions.

REFERENCES

- [1] A. Dudek, Archives of Metallurgy and Materials **56**, 135-140 (2011).
- [2] B. Zboromirska-Wnukiewicz, J. Wnukiewicz, K. Kogut, K. Kasprzyk, W. Wnukiewicz, Archives of Metallurgy and Materials **54**, 1005-1011 (2009).
- [3] M. Rozmus, J. Kusiński, M. Blicharski, J. Marczyk, Archives of Metallurgy and Materials **54**, 665-670 (2009).
- [4] E. Mitura, S. Mitura, P. Niedzielski, Z. Has, R. Wolowicz, A. Jakubowski, J. Szmidt, A. Sokolowska, P. Louda, J. Marciniak, B. Koczy, Diamond and Related Materials **3**, 896-898 (1994).
- [5] S. Mitura, A. Mitura, P. Niedzielski, P. Couvrat, Chaos, Solitons and Fractals **10**, 2165-2176 (1999).
- [6] J. Grabarczyk, D. Batory, P. Louda, P. Couvrat, I. Kotela, K. Bakowicz-Mitura, Journal of Achievements in Materials and Manufacturing Engineering **20**, 107-110 (2007).
- [7] Z. Paszenda, J. Tyrlik-Held, W. Jurkiewicz, Journal of Achievements in Materials and Manufacturing Engineering **31/2**, 348-355 (2008).
- [8] K. Perzyński, Ł. Major, Ł. Madej, M. Pietrzyk, Archives of Metallurgy and Materials **56**, 393-399 (2011).
- [9] A. Grill, IBM Journal of Research and Development **43**, 147-161 (1999).
- [10] Y. Catherine, in Diamond and Diamondlike Films and Coatings, NATO-ASI Series B: Physics, Clausing R. E., Horton L.L., Angus J.C., and Koidl P., Eds., Plenum Publishing Co., New York, 1991, p. 193.
- [11] S. Mitura, Journal of Crystal Growth **80**, 417-424 (1987).
- [12] M.A. Tamor, W.C. Vassell, K.R. Carduner, Applied Physics Letters **58**, 592-594 (1991).
- [13] P.C.T. Ha, D.R. McKenzie, M.M.M. Bilek, E.D. Doyle, D.G. McCulloch, P.K. Chu, Surface and Coatings Technology **200**, 6405-6408 (2006).
- [14] Z. Has, S. Mitura, M. Cłapa, J. Szmidt, Thin Solid Films **136**, 161-166 (1986).
- [15] S. Mitura, Z. Has, V.I. Gorokhovskiy, Surface and Coatings Technology **47**, 106-112 (1991).
- [16] J.R. Woodworth, M.E. Riley, D.C. Meister, B.P. Aragon, M.S. Le, H.H. Sawin, Journal of Applied Physics **80**, 1304-1311 (1996).
- [17] A. Von Keudell, W. Jacob, Journal of Applied Physics **79** (2), 1092-1098 (1996).
- [18] Y. Sun, T. Bell, Wear **253**, 689-693 (2002).
- [19] M. Tsujikawa, D. Yoshida, N. Yamauchi, N. Uedac, T. Sonce, S. Tanakad, Surface and Coatings Technology **200**, 507-511 (2005).
- [20] Y. Sun, Journal of Materials Processing Technology **168**, 189-194 (2005).